First-principles studies of ground-state and dynamical properties of MgS, MgSe, and MgTe in the rocksalt, zinc blende, wurtzite, and nickel arsenide phases

S. Duman,[1] S. Bağcı,[1] H. M. Tütüncü,[1,2] and G. P. Srivastava[2]
[1]*Sakarya Üniversitesi, Fen-Edebiyat Fakültesi, Fizik Bölümü, Esentepe, 54140 Adapazarı, Turkey*
[2]*School of Physics, University of Exeter, Stocker Road, Exeter EX4 4QL, United Kingdom*
(Received 23 November 2005; revised manuscript received 20 March 2006; published 9 May 2006)

An *ab initio* pseudopotential method is used to investigate the structural and electronic properties of MgS, MgSe, and MgTe in the rocksalt, zinc blende, wurtzite, and nickel arsenide phases. It is found that rocksalt is the most stable phase for MgS and MgSe, while nickel arsenide is the most stable phase for MgTe. Differences in the density of states for the upper valence bands and lower conduction bands between these competing phases are pointed out. The lattice dynamics of these semiconductors has been studied by employing a linear response approach based on the density functional theory. Differences in the phonon spectra and density of states both in the acoustic and optical ranges between the competing phases are investigated. The calculated zone-center phonon modes for the rocksalt and zinc blende phases of MgS are in good agreement with experimental observations.

DOI: 10.1103/PhysRevB.73.205201 PACS number(s): 63.20.Dj, 71.15.Mb, 71.20.Nr

I. INTRODUCTION

In recent years Mg chalcogenides have attracted both scientific and technological interest. There are several reasons for studying these semiconductors. Due to their large band gaps and low dielectric constants, they can be used in blue- and ultraviolet-wavelength optics and high-temperature electronics.[1–4] Moreover, these semiconductors are also a potentially very good choice for protective coatings due to their hardness, high melting point, high thermal conductivity, and large bulk modulus. These semiconductors are known to exist in four crystalline phases: rocksalt, zinc blende, wurtzite, and nickel arsenide. It is therefore important to accurately determine the structural, electronic, vibrational, and thermal properties in order to assess the relative importance of these four phases.

The lattice constants of the rocksalt (RS) and zinc blende (ZB) MgS, MgSe, and MgTe have been measured by several experimental groups.[5–7] For the wurtzite (WZ) and nickel arsenide (NiAs) phases, all three independent structural parameters (c, a, and the internal cell parameter u) have been obtained experimentally.[8–10] On the theoretical side, the ground-state and electronic properties have been determined as follows: all four phases of MgSe and MgTe by Camp *et al.*;[11] the RS and NiAs phases of the three materials by Chakrabarti;[12] the RS, ZB, and WZ phases of MgS and MgSe by Rached *et al.*;[13] and the RS and ZB phases of all three materials by Drief *et al.*[14] The effect of a quasiparticle calculation on the band gaps of the ZB phase of MgSe and MgTe was discussed by Fleszar.[15] The energy difference between the ZB and WZ polytypes of MgTe was carefully determined by Yeh *et al.*[16]

Despite much work on the structural and electronic properties of these semiconductors, the dynamical properties of the four phases are relatively poorly known in the literature. A wide variety of physical properties of solids depend on their phonon properties, such as specific heats, thermal expansion, heat conduction, and electron-phonon interaction. Phonon dispersion curves are typically obtained by the neutron-scattering technique. However, due to difficulty in preparing large group II-VI single crystals, this technique has not yet been successfully applied. In addition to this technique, Raman and infrared spectroscopies can be used to study phonon modes in semiconductors. Measurements of zone-center phonon modes, using the Raman spectroscopy technique,[17,18] in the zinc blende phase of MgS and MgSe have been presented. Infrared spectroscopy[19] has been used to determine the zone-center phonons of rocksalt MgS. However, phonons have not yet been measured experimentally for any phase of MgTe. Few theoretical works are available for phonons in these semiconductors. A first-principles method, within the density functional theory,[17] has been used to obtain the zone-center frequencies of the zinc blende MgS. In addition to this theoretical work, these zone-center phonon modes have been calculated using a three-body force potential.[20] However, phonon dispersion curves for any phases of these semiconductors have not been studied by using any theoretical methods.

Thus it is clear that there are no reports from a single research group, theoretical or experimental, on a comparative study of any property for the four phases of the three materials. Such a study seems important, especially in view of the energy closeness of some of the phases. For example, the available density functional results by Yeh *et al.*[16] suggest that there is only a difference of 1 meV/(per atom) between the ZB and WZ phases of MgTe, an energy difference which lies at the edge of the present day theoretical accuracy limit. The following question, then, is pertinent: can we point out any significant differences in the electronic or vibrational properties, if any two phases of a given Mg chalcogenide that cannot be separated on grounds of the total energy difference?

In an attempt to resolve some of the above uncertainties,

we have in this paper undertaken a systematic *ab initio* theoretical study of the ground state, electronic band structure, and phonon dispersion relations of the four phases of the three Mg chalcogenides. To investigate the structural and electronic properties, we performed *ab initio* pseudopotential calculations within the local density approximation of the density functional theory. These results are used to further calculate the phonon spectra by employing a linear response technique based on the density functional perturbation theory. An attempt is made to extract meaningful trends in such properties across the Mg chalcogenides.

II. METHOD OF CALCULATION

We used the plane-wave pseudopotential approach within the framework of density functional theory. The *ab initio* norm-conserving pseudopotentials were generated using the method of Troullier and Martins.[21] The electron-electron interaction was considered within the local density approximation (LDA) of the density functional theory, with the correlation scheme of Ceperley and Alder.[22] The electronic wave functions were expanded in a basis set of plane waves, up to a kinetic energy cutoff of 50 Ry for all the considered wide-gap semiconductors. For the **k**-point sampling, we use 56, 56, 60, and 75 special points in the irreducible wedge of the Brillouin zone of the rocksalt, zinc blende, wurtzite, and nickel arsenide structures, respectively. For all the considered phases, the Kohn-Sham equations were solved using an iterative conjugate gradient scheme to find the total energy. These considerations allow total energies of competing phases to be compared within an accuracy of at least 2 meV/atom.

Having obtained self-consistent solutions of Kohn-Sham equations, the lattice-dynamical properties were calculated within the framework of the self-consistent density functional perturbation theory.[23,24] In order to obtain full phonon spectrum we evaluated 16 dynamical matrices on a $6\times6\times6$ grid in **q** space for the rocksalt and zinc blende phases, 24 matrices (on a $4\times4\times4$ grid) for the wurtzite phase, and 21 matrices (on a $4\times4\times4$ grid) for the nickel arsenide phase. These dynamical matrices were Fourier transformed to obtain the phonon dispersion curves and density of states. We estimate that the convergence of phonon frequencies is within 3 cm^{-1} for the chosen kinetic energy cutoff and the special **k** points. All the calculations have been performed by using the code PWSCF.[25]

III. RESULTS

A. Structural properties

The equilibrium lattice parameters (viz., the cubic lattice constant a for the RS and ZB structures and the hexagonal lattice constant a, ratio c/a, and internal parameter u for the WZ and NiAs structures) were determined by fitting the calculated total energy results as functions of the reduced atomic volume (V/V_0) using the Murnaghan equation of state.[26] For the hexagonal close-packed phases we minimized the total energy with respect to c/a and u for a chosen unit cell volume $V=\sqrt{3}a^2c/2$. The total energy results are shown in Fig. 1 and Table I. In agreement with experimental[27,28] and previous theoretical[11,13,14,29,30] works, we find that the ground-state phase of MgS and MgSe is the RS structure. Also, in agreement with experimental[10] and previous theoretical[11,12,14,30] calculations, we find that the NiAs phase is the ground-state structure for MgTe. It is interesting to

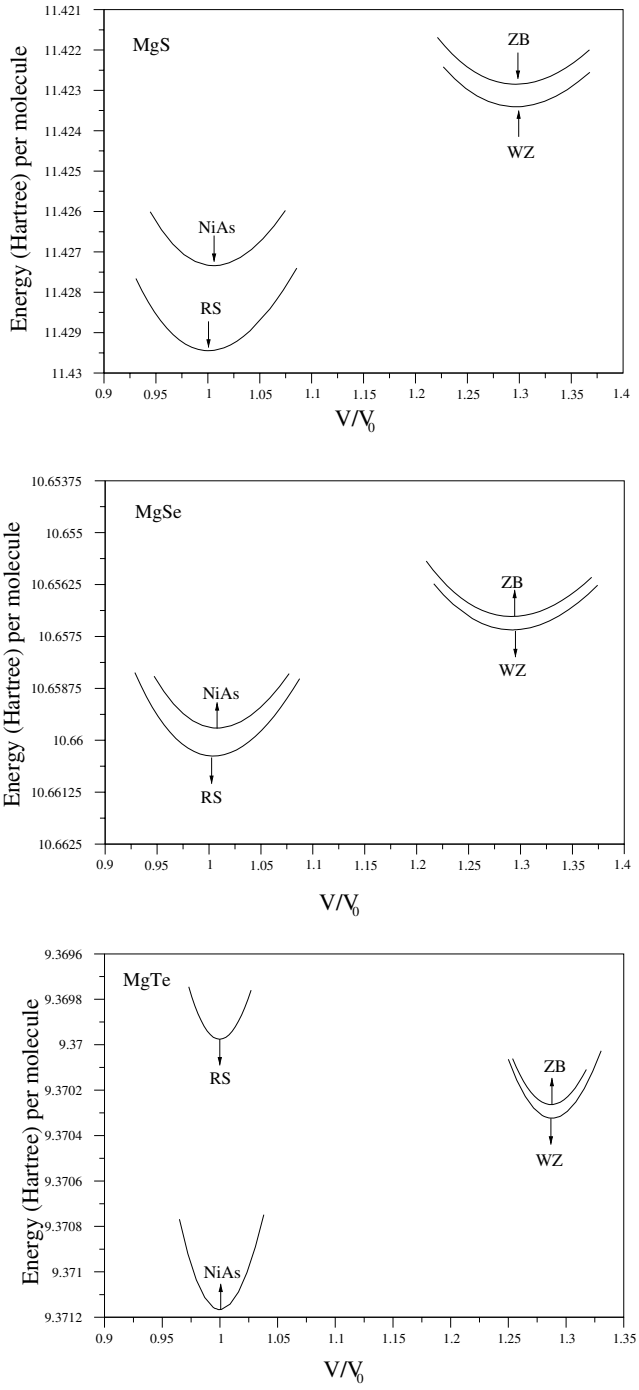

FIG. 1. Calculated total energies as a function of the fractional volume (V/V_0). V_0 is the equilibrium volume of the ground-state phase. For MgS and MgSe, the ground-state phase is the rocksalt structure while the nickel arsenide structure is the ground-state phase for MgTe.

TABLE I. Comparison of total energy differences (meV/atom) for MgS, MgSe, and MgTe in the rocksalt (RS), zinc blende (ZB), wurtzite (WZ), and nickel arsenide (NiAs) phases. The ground-state energy is set to zero.

	MgS		MgSe		MgTe		
	Present	Ref. 12	Present	Ref. 12	Present	Ref. 12	Ref. 16
RS	0.0	0.0	0.0	0.0	16	22	13.7
ZB	90		46		13		15
WZ	82		41		12		14
NiAs	29	68	9	14	0.0	0.0	0.0

note that MnTe (Ref. 31) has also an atomic arrangement in the NiAs structure. The similarity of the ground state phase of MgTe and MnTe can be related to Te atoms.

Our structural results for all the considered phases of MgS, MgSe, and MgTe are listed in Tables II and III. From these tables, it has been found that the values of B and B' for the WZ structure are similar to their corresponding values for the ZB structure. The reason for this similarity is that these structures have similar tetrahedral bonds up to the second neighbors, rendering the energy differences between these two structures very small (see also Table I). It should be mentioned that in the WZ structure, the straight bond in the [001] direction is slightly longer than other three (slanted) bonds. The calculated values of macroscopic dielectric tensor ε_∞ and the Born effective charge Z^B for this structure are presented along and perpendicular to the c axis in Table III. Although the structural similarity between NiAs and RS structures is not as close as that between the ZB and WZ phases, these structures can be related to each other. The similarity between these structures is that each cation has the same octahedral environment for both phases. As a result of this similarity, the dielectric constants and effective charges for both structures are very close to each other, as seen in Tables II and III.

From an inspection of the results in Table I, we make three observations. First, the energy difference between ground state and the next energy phase decreases across the anionic sequence S-Se-Te. Second, for all three materials, the energy difference between the ZB and WZ phases is very small: 1, 5, and 8 meV/(per atom) for MgTe, MgSe, and MgS, respectively. Third, all four crystal phases of MgTe equilibrate within a small energy difference of 16 meV/(per atom). The special case of MgTe was highlighted earlier by Yeh *et al.*,[16] who using a linearized augmented-plane-wave method, obtained results very similar to what is reported in this work. As the energy difference of 1 meV/(per atom) between the ZB and WZ phases for MgTe, obtained both in this work as well in Ref. 16, is within the present day computational accuracy limit, an examination of other properties is required to find any fingerprints of these two crystal phases. This will be attempted in the next two sections.

B. Electronic properties

The electronic band structures and density of states of the Mg chalcogenides, calculated within the LDA, for the RS,

TABLE II. Calculated structural parameters of MgS, MgSe, and MgTe in the RS and ZB structures. The obtained results are also compared with previous experimental and theoretical results.

II–VI (structure)	a (Å)	B (Mbar)	B'	ε_∞	Z^B
MgS (RS)	5.18	0.81	4.15	5.66	2.35
Theory[a]	5.14	0.92	4.44		
Theory[b]	5.14	0.82	3.98	5.81	
Experimental[c]	5.19				
MgSe (RS)	5.46	0.65	3.90	6.83	2.48
Theory[a]	5.40	0.74	3.52		
Theory[b]	5.40	0.68	4.15	6.85	
Experimental[d]	5.46				
MgTe (RS)	5.90	0.51	4.35	9.20	2.76
Theory[e]	5.92	0.54	4.04		
Theory[b]	5.86	0.52	4.10	9.26	
Experimental[f]	6.02				
MgS (ZB)	5.64	0.60	4.06	4.24	1.91
Theory[a]	5.61	0.60	3.89		
Theory[b]	5.61	0.61	4.06	4.50	
Experimental[g]	5.66				
MgSe (ZB)	5.92	0.49	3.75	4.87	1.91
Theory[a]	5.89	0.54	4.27		
Theory[b]	5.88	0.50	4.02	5.16	
Experimental[h]	5.89				
MgTe (ZB)	6.39	0.38	3.79	5.72	1.93
Theory[e]	6.44	0.38	3.96		
Theory[b]	6.38	0.38	3.89	6.09	
Experimental[i]	6.36				

[a]Reference 13.
[b]Reference 14.
[c]Reference 27.
[d]Reference 28.
[e]Reference 11.
[f]Reference 36.
[g]Reference 7.
[h]Reference 5.
[i]Reference 6.

TABLE III. Calculated structural parameters of MgS, MgSe, and MgTe in the WZ and NiAs structures. The obtained results are also compared with previous experimental and theoretical results.

II–VI (structure)	a (Å)	c (Å)	B (Mbar)	B'	u	$\varepsilon_\perp(\infty)$	$\varepsilon_\parallel(\infty)$	$Z^B_\perp$	$Z^B_\parallel$
MgS (WZ)	3.996	6.492	0.63	4.18	0.3777	4.20	4.31	1.89	1.97
Theory[a]	3.945	6.443	0.57	4.10					
Theory[b]	3.969	6.487	0.64	2.96					
Experimental[c]	3.972	6.443							
MgSe (WZ)	4.196	6.825	0.50	3.78	0.3770	4.82	4.94	1.88	1.97
Theory[d]	4.237	6.836	0.50	3.94	0.3785				
Theory[b]	4.165	6.799	0.52	4.31					
Experimental[e]	4.145	6.723							
MgTe (WZ)	4.531	7.381	0.38	4.04	0.3762	5.67	5.78	1.89	1.98
Theory[d]	4.530	7.405	0.43	3.82	0.3751				
Theory[f]	4.503	7.355	0.42	4.31					
Experimental[g]	4.540	7.386							
Experimental[h]	4.548	7.394							
MgS (NiAs)	3.605	6.092	0.82	4.15	0.25	5.59	5.63	2.22	2.28
Theory[i]	3.598	5.995							
MgSe (NiAs)	3.819	6.367	0.67	4.15	0.25	6.78	6.79	2.34	2.39
Theory[d]	3.866	6.471	0.65	4.11					
Theory[i]	3.809	6.248	0.63	3.96					
MgTe (NiAs)	4.158	6.768	0.53	4.28	0.25	9.16	9.35	2.57	2.60
Theory[d]	4.183	6.841	0.58	3.89					
Theory[i]	4.127	6.723	0.48	3.47					
	4.029	6.563	0.61	4.13					

[a]Reference 29.
[b]Reference 13.
[c]Reference 36.
[d]Reference 11.
[e]Reference 9.
[f]Reference 37.
[g]Reference 6.
[h]Reference 10.
[i]Reference 12.

ZB, WZ, and NiAs structures are presented in Figs. 2–5 respectively. Numerical values of the band gaps at various symmetry points are given in Tables IV and V. While the ZB and WZ phases are characterized with a direct band gap, the RS and NiAs phases are characterized with an indirect band gap. The magnitude of the direct band gap (at zone center) is slightly smaller for the ZB phase than for the WZ phase. The indirect band gap (along Γ-X) for the RS phase is slightly smaller than the indirect band gap (along Γ-K) for the NiAs phase. For all the three Mg chalcogenides the lowest band occurs for the RS phase. In general, our band gap results from calculations along various symmetry directions are in agreement with available previous works along fewer symmetry directions. Experimental results of the band gap are available for the ZB phase and are listed in Table IV. The well-known band gap reduction of our LDA band gap result for the ZB phase, compared to experimental measurements, is approximately 30% for all three chalcogenides. It is expected that quasiparticle calculations would bring the band gap values in close agreement with the experimental results. Quasiparticle calculations[15,32] indicate that for semiconductors with s and p valence electrons the change in the band gap is almost a constant at least at the principal symmetry points in the Brillouin zone. Thus we expect that good agreement between theoretically and experimentally measured band gaps can be easily established by making an adequate shift of the presently calculated band gap results. Table IV indicates that an upward shift of approximately 1.2 eV would bring the presently obtained LDA band gaps near the experimentally determined values for the ZB phase.

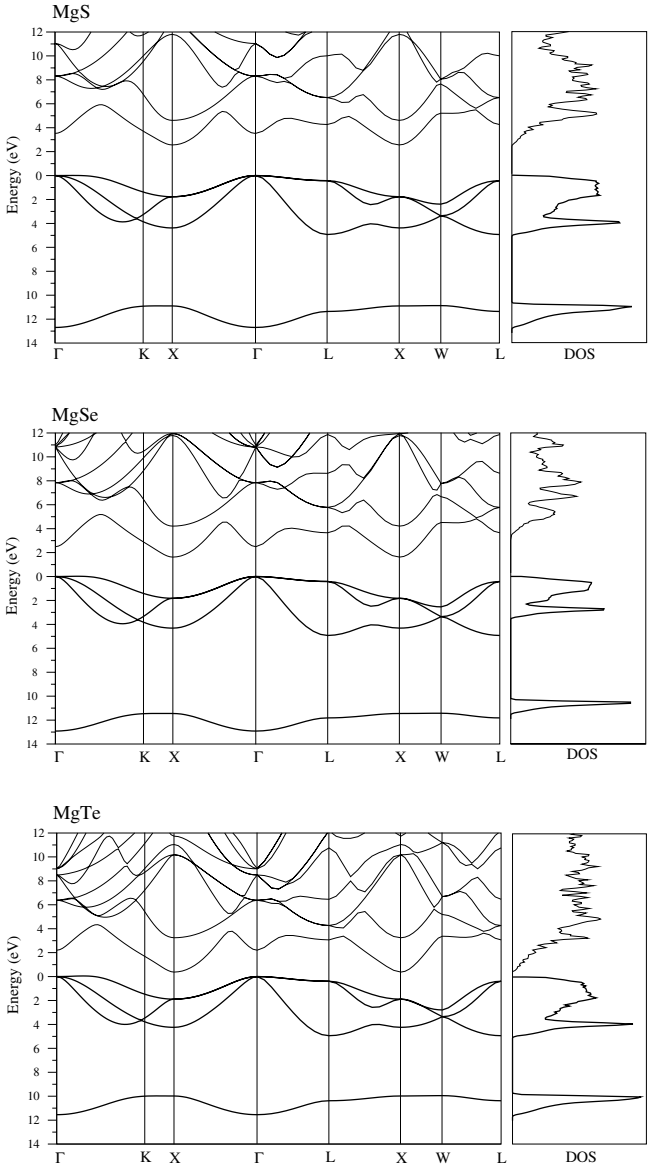

FIG. 2. Calculated electronic band structures and total density of states for Mg chalcogenides in the rocksalt structure.

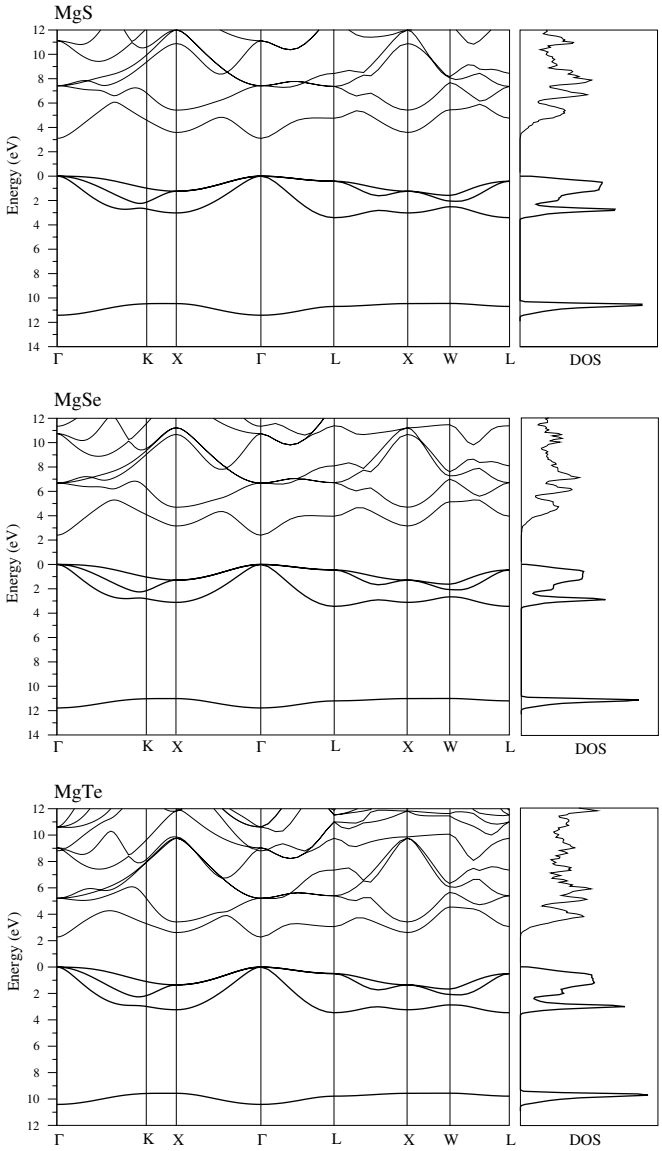

FIG. 3. Calculated electronic band structures and total density of states for Mg chalcogenides in the zinc blende structure.

We can observe a few trends in the electronic density of states. For each of the Mg chalcogenides the valence band widths of the ZB and WZ structures are slightly smaller than the valence band width of the RS and NiAs structures. The valence band for the RS and ZB structures with two atoms per unit cell is characterized with a sharp *s* peak, a sharp *sp* peak, and a broad *p* peak. The valence bands of the WZ and NiAs structures with four atoms per unit cell show broadened and structured *s*, *sp*, and *p* bands.

C. Dynamical properties

We will discuss characteristic details of the phonon dispersion curves for each of the phases in separate subsections.

1. Rocksalt phase

Figure 6 shows the dispersion curves and density of states for Mg chalcogenides in the RS phase. These phonon dispersion curves show one important feature of ionic crystals—namely, that the longitudinal optic (LO) and transverse optic (TO) phonon modes are split at the zone center. For MgS our calculated results for the TO and LO modes at the zone center are 241 cm^{-1} and 397 cm^{-1}, respectively. These values compare very well with experimentally measured value[19] of 245 cm^{-1} (TO) and 390 cm^{-1} (LO), respectively. Our calculated value of the zone-center LO-TO splitting is 156 cm^{-1}, 121 cm^{-1}, and 96 cm^{-1} for MgS, MgSe, and MgTe, respectively. The LO phonon branch shows a large amount of dispersion along the [100] and [110] directions for all three RS semiconductors (see Fig. 6). This behavior can be related to the atomic arrangement and atomic bondings in the RS structure. Similar observations have been made in the lattice dynamics of Pb chalcogenides.[33] The LO phonon mode of the NaCl crystal also shows a large amount of dispersion along these symmetry directions.[34] Due to only a small mass difference between Mg and S atoms, there is no clear gap be-

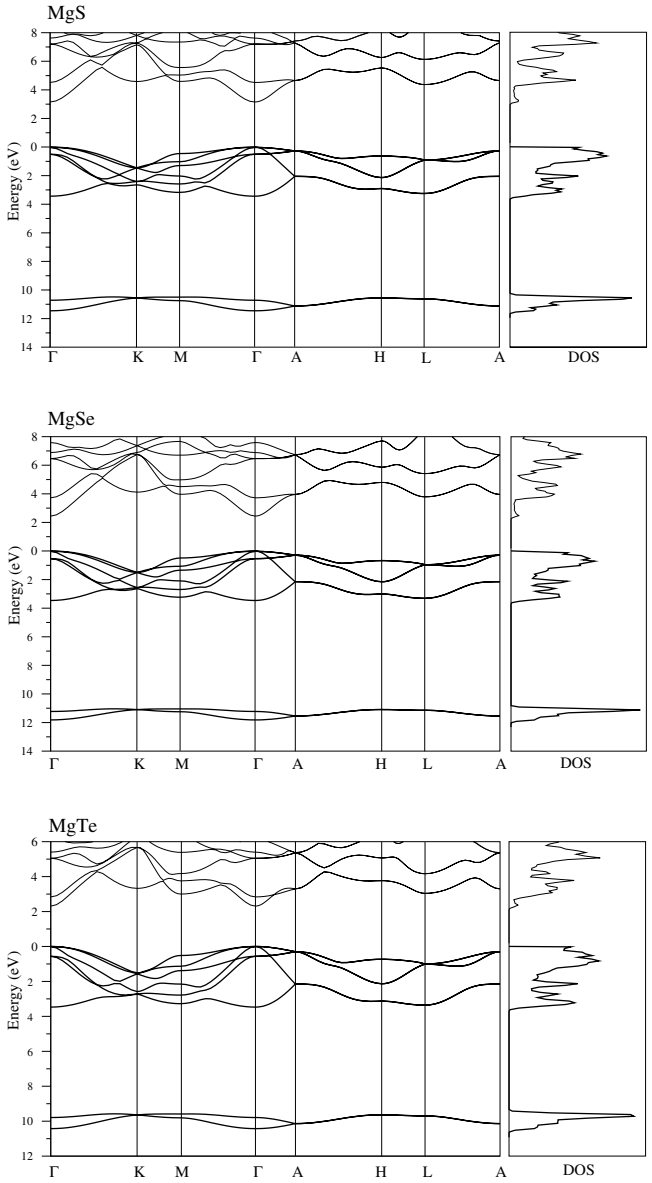

FIG. 4. Calculated electronic band structures and total density of states for Mg chalcogenides in the wurtzite structure.

tween the acoustic and optic branches for the RS MgS. This observation can also be seen in the phonon density of states for this semiconductor. Moreover, the frequency localization of longitudinal acoustic (LA) phonon branch along the [111] direction for this semiconductor is different from that of the RS MgSe and MgTe. For large-**q** wave vectors along this symmetry direction the LA phonon branch lies higher in energy than the TO phonon branch for the RS MgS. This kind of behavior has been observed in the phonon spectra of the NaCl crystal.[34] At the *L* points the frequencies are 177 cm^{-1} transverse acoustic (TA), 207 cm^{-1} (TO), 293 cm^{-1} (LA), and 364 cm^{-1} (LO). Figure 7 presents a schematic illustration of the eigendisplacements of the TA, LA, TO, and LO phonon modes for this semiconductor at the *L* point. Because of the mass difference between Mg and S atoms, the acoustic and optical phonon modes are characterized by the motion of S and Mg atoms, respectively.

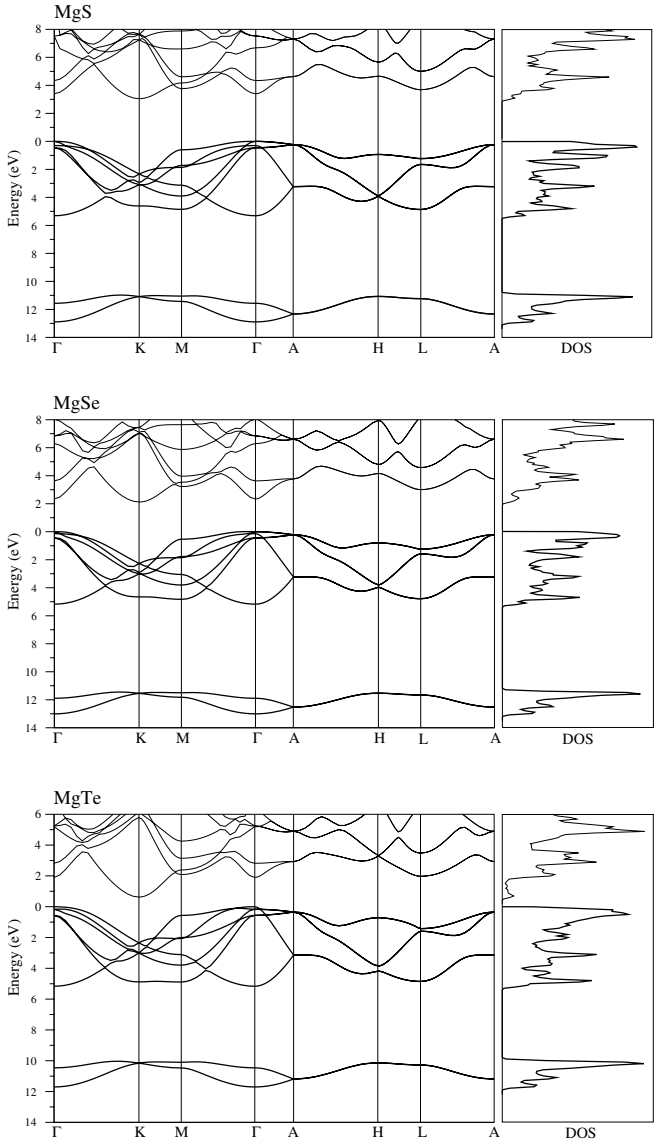

FIG. 5. Calculated electronic band structures and total density of states for Mg chalcogenides in the nickel arsenide structure.

For the RS MgSe and MgTe, there is a clear optical-acoustic band gap in the phonon dispersion curves due to a larger cation/anion mass ratio. The TO phonon branch in these semiconductors shows a smaller extent of dispersion than the corresponding phonon branch in the RS MgS. These changes are manifested in a sharp peak in the phonon density of states of the RS MgSe and MgTe.

2. Zinc blende phase

The phonon dispersion curves and density of states of MgS, MgSe, and MgTe in the ZB phase are plotted in Fig. 8. For this structure, we have calculated the zone-center TO (LO) phonon modes with frequencies 341 cm^{-1} (429 cm^{-1}) for MgS, 274 cm^{-1} (337 cm^{-1}) for MgSe, and 243 cm^{-1} (288 cm^{-1}) for MgTe. The calculated TO (LO) frequencies for MgS and MgSe are in good agreement with the experimental values of 327 ∓ 6 cm^{-1} (425 ∓ 1 cm^{-1}) for MgS (Ref.

TABLE IV. The calculated electronic band gaps (in eV) for the RS and ZB phases of Mg chalcogenides and their comparison with other theoretical and experimental results.

Material (structure)	Reference	Direct (at Γ)	Direct (at *X*)	Direct (at *L*)	Indirect (Γ-*X*)	Indirect (Γ-*L*)
MgS (RS)	This work	3.52	4.33	4.70	2.56	4.27
	Tight binding[a]	3.60	4.60	5.50	2.70	4.7
	Ab initio[b]				2.21	
	Ab initio[c]				2.69	
MgSe (RS)	This work	2.50	3.44	4.10	1.62	3.65
	Tight binding[a]	2.50	3.50	4.70	1.5	3.90
	Ab initio[b]				1.95	
MgTe (RS)	This work	2.20	2.27	3.46	0.38	3.07
	Ab initio[b]				0.41	
MgS (ZB)	This work	3.10	4.82	5.18	3.59	4.76
	Tight binding[a]				3.70	
	Ab initio[d]	3.42			3.64	5.03
	Ab initio[b]	3.37				
	Experiment[e]	4.50				
MgSe (ZB)	This work	2.40	4.45	4.41	3.16	3.97
	Tight binding[a]				3.30	
	Tight binding[d]	2.82			3.27	
	Ab initio[b]	2.82				
	Ab initio[f]	2.47			3.11	4.03
	Experiment[g]	3.60				
MgTe (ZB)	This work	2.27	3.96	3.56	2.61	3.10
	Ab initio[b]	2.61				
	Ab initio[f]	2.29			2.38	2.99
	Experiment[h]	3.47				

[a]Reference 38.
[b]Reference 14.
[c]Reference 39.
[d]Reference 40.
[e]Reference 41.
[f]Reference 15.
[g]Reference 5.
[h]Reference 42.

17) and 237 cm^{-1} (340 cm^{-1}) for MgSe (Ref. 18). Our calculated TO (LO) frequencies for MgS also compare very well with previous *ab initio* results of 336 cm^{-1} (428 cm^{-1}) (Ref. 17) and a three-body force potential results of 319 cm^{-1} (414 cm^{-1}) (Ref. 20).

In contrast to the RS MgS, the optical-acoustic band gap does exist for the ZB phase of this semiconductor (see Figs. 6 and 8). In particular, the frequency difference between TO and LA phonon modes is found to be 54 cm^{-1} at *X* and 66 cm^{-1} at *L* for the ZB MgS. We believe that the main source of the difference for the optical-acoustic gap between the RS and ZB phases is the tetrahedral bonds in the latter structure. A second difference in the phonon spectrum between these two structures is the dispersion behavior of TO phonon branch along the main high-symmetry directions ([100] and [111]). This branch is nearly flat for the ZB phase. Thus, there is a clear development of the TO peak in the density of states for the ZB MgS, MgSe, and MgTe.

3. Wurtzite phase

Complete phonon branches and phonon density of states are plotted for the WZ MgS, MgSe, and MgTe in Fig. 9. Due to four atoms per unit cell in the WZ structure, there are 12 vibrational modes for any **q** point (see Fig. 9). However, there are only eight distinct phonon branches along the Γ-*A* (Δ) symmetry direction, due to the degeneracy of four lon-

TABLE V. The calculated electronic band gaps (in eV) for the WZ and NiAs phases of Mg chalcogenides and their comparison with other theoretical results.

Material (structure)	Reference	Direct (at Γ)	Direct (at *K*)	Direct (at *M*)	Indirect (Γ-*K*)	Indirect (Γ-*M*)	Indirect (Γ-*L*)
MgS (WZ)	This work	3.15	6.04	5.05	4.58	4.59	4.36
	Ab initio[a]	3.50					
MgSe (WZ)	This work	2.44	5.61	4.45	4.11	3.96	3.78
	Ab initio[a]	2.61					
MgTe (WZ)	This work	2.31	4.83	3.52	3.32	3.00	3.04
MgS (NiAs)	This work	3.40	5.38	4.36	3.05	3.76	3.69
MgSe (NiAs)	This work	2.34	4.39	3.75	2.12	3.22	3.00
MgTe (NiAs)	This work	1.90	2.97	2.65	0.63	2.09	1.98
	Ab initio[b]	2.35			0.81	2.41	2.05

[a]Reference 13.
[b]Reference 11.

gitudinal and four transverse modes. Moreover, only four phonon modes are found at the *A* point due to two doubly degenerate longitudinal modes and two fourfold-degenerate transverse modes. Also note that the second and third branches along the Γ-*A* direction repel each other as they approach each other in frequency. This is known as the *anticrossing* effect between two states of the same symmetry.[35] We have observed six phonon branches along the high symmetry directions *A*-*H*, *H*-*L*, and *L*-*A*. Along the least symmetry directions Γ-*K* and Γ-*M*, the 12 phonon branches are in general nondegenerate. The highest optical phonon mode for these semiconductors shows a reasonable amount of dispersion along these least symmetry directions. The calculated width of the dispersion of this phonon branch is found to be 90 cm^{-1} (88 cm^{-1}), 53 cm^{-1} (31 cm^{-1}), and 34 cm^{-1} (17 cm^{-1}) for MgS, MgSe, and MgTe along the Γ-*K* (Γ-*M*) symmetry direction. These results clearly indicate that the highest optical branch in MgTe shows less dispersion than its counterpart for MgS and MgSe. The influence of the large mass difference between Te and Mg atoms is reflected in the fact that this phonon branch is characterized by the vibrations of Mg atoms in the isotropic field of intratetrahedral forces. Thus, this phonon branch in MgTe shows smaller dispersion compared to the corresponding branch in MgS and MgSe. The flatness of the highest phonon modes for MgSe and MgTe along the *L*-*A* symmetry direction creates sharp peaks with frequencies of 310 cm^{-1} and 280 cm^{-1} in the phonon density of states. However, this peak has not been observed in the phonon density of states of MgS due to the relatively large dispersion of the highest optical branch along all the symmetry directions. Along the *A*-*H* and *L*-*A* directions, the first and second phonon branches above the gap regions display small dispersions. Due to this, there are clear peaks in the density of states with frequencies of 335 cm^{-1} for MgS, 265 cm^{-1} for MgSe, and 230 cm^{-1} for MgTe. Below the gap region, we have observed two clear

TABLE VI. The calculated zone center frequencies (cm^{-1}) for WZ and NiAs MgS, MgSe, and MgTe.

Mg chalcogenides (structure)	E_2^1	B_1^1	A_1(TO)	E_1(TO)	E_2^2	B_1^2	A_1(LO)	E_1(LO)
MgS(WZ)	89	259	324	344	326	338	403	443
MgSe(WZ)	53	163	266	276	271	294	332	336
MgTe(WZ)	36	117	239	244	238	265	286	288
MgS (NiAs)	182	212	260	415	271	293	404	408
MgSe(NiAs)	127	164	196	370	170	215	304	314
MgTe(NiAs)	96	121	162	309	152	189	245	266

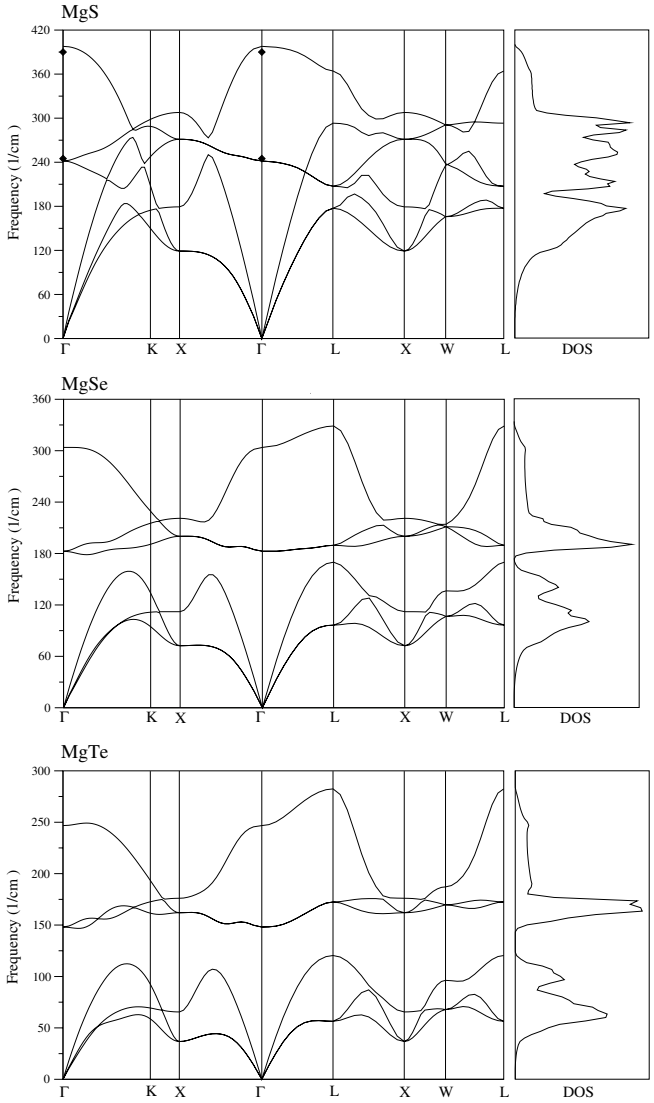

FIG. 6. *Ab initio* phonon dispersions and density of states for MgS, MgSe, and MgTe in the rocksalt structure. Experimental data (solid diamonds) for MgS are taken from Ref. 19.

peaks for these semiconductors. The higher-frequency one can be linked to the flatness of the third phonon branch along the *H*-*L* direction while the lower-frequency one is due to acoustic phonon modes.

For the WZ structure with C_{6v} point group symmetry, group theory predicts the following zone-center optical modes: $2A_1+2B_1+2E_1+2E_2$. The A_1 and E_1 optic modes are both Raman and infrared active, and the E_2 mode is only Raman active, while the B_1 mode is silent. Furthermore, the A_1 and E_1 phonon modes split into LO and TO components due to the macroscopic electric field associated with the atomic displacements of the longitudinal optical phonons. The calculated zone-center phonon frequencies for WZ MgS, MgSe, and MgTe are given in Table VI. In general, the frequency of the E_1(LO) mode for the WZ structure is quite close to the LO mode frequency for the ZB structure.

The variations of the frequencies of A_1(TO) and A_1(LO) phonon modes against the square root of the inverse reduced

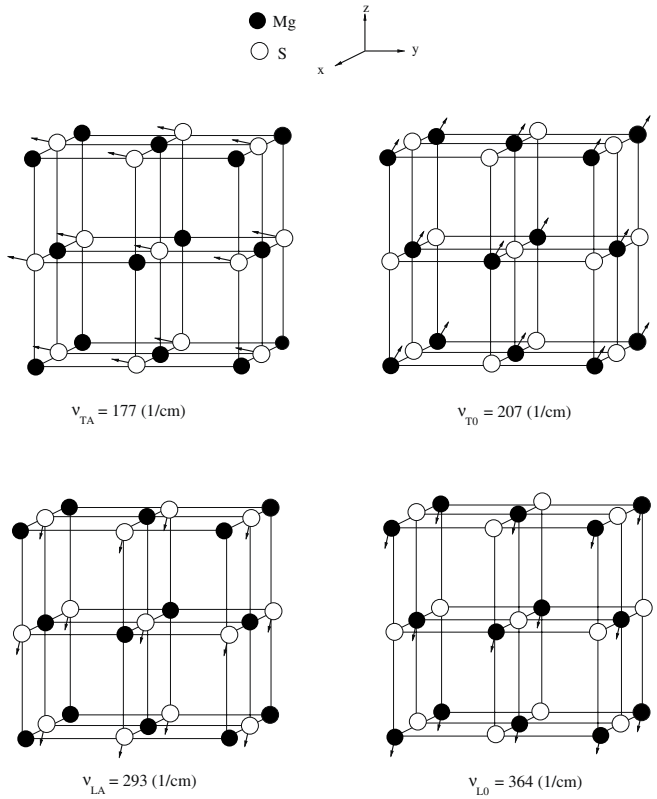

FIG. 7. Eigenvectors representations of TA, LA, TO, and LO phonon modes for the rocksalt MgS at the *L* point.

mass of the cation and anion are illustrated in Fig. 10. Clearly these phonon modes show a nearly linear increase with the inverse reduced mass along the sequence MgTe-MgSe-MgS, indicating a very similar effective force constant for these materials. Such a variation has also been observed for the E_1(TO) and E_1(LO) phonon modes of these semiconductors. As a result of the anisotropic nature of the WZ structure, these modes have an angular dependence. Figure 11 displays the angular dispersion of the zone-center phonon frequencies of WZ Mg chalcogenides. As can be seen from this figure, the zone-center LO and TO frequencies show angular dispersion with respect to the *c* axis. For all the considered Mg chalcogenides, the A_1(LO) and E_1(TO) phonon modes turn into E_1(LO) and A_1(TO) phonon modes when θ goes from 0 to 90°. However, for values of θ intermediate between 0 and 90° the modes are mixed and do not acquire pure LO or TO character or A_1 or E_1 symmetry. The width E_1(LO)-A_1(LO) [E_1(TO)-A_1(TO)] is found to be 40 cm^{-1} [20 cm^{-1}], 4.0 cm^{-1} [10 cm^{-1}], and 2.0 cm^{-1} [5.0 cm^{-1}] for MgS, MgSe, and MgTe, respectively. Compared to their ZB structures, these values are very small. This comparison shows that the anisotropy due to the long-range electrostatic forces is much smaller for the WZ phase of these semiconductors. The crystal anisotropy factor $[\omega(E_1(\mathrm{TO}))-\omega(A_1(\mathrm{TO}))]/\omega(E_1(\mathrm{TO}))$ is calculated to be 0.056, 0.037, and 0.023 for MgS, MgSe, and MgTe, respectively. From these results, one can say that MgS is more anisotropic than MgSe and MgTe. However, the zone-center B_1^2 and E_2^2 optical phonon modes do not show any appre-

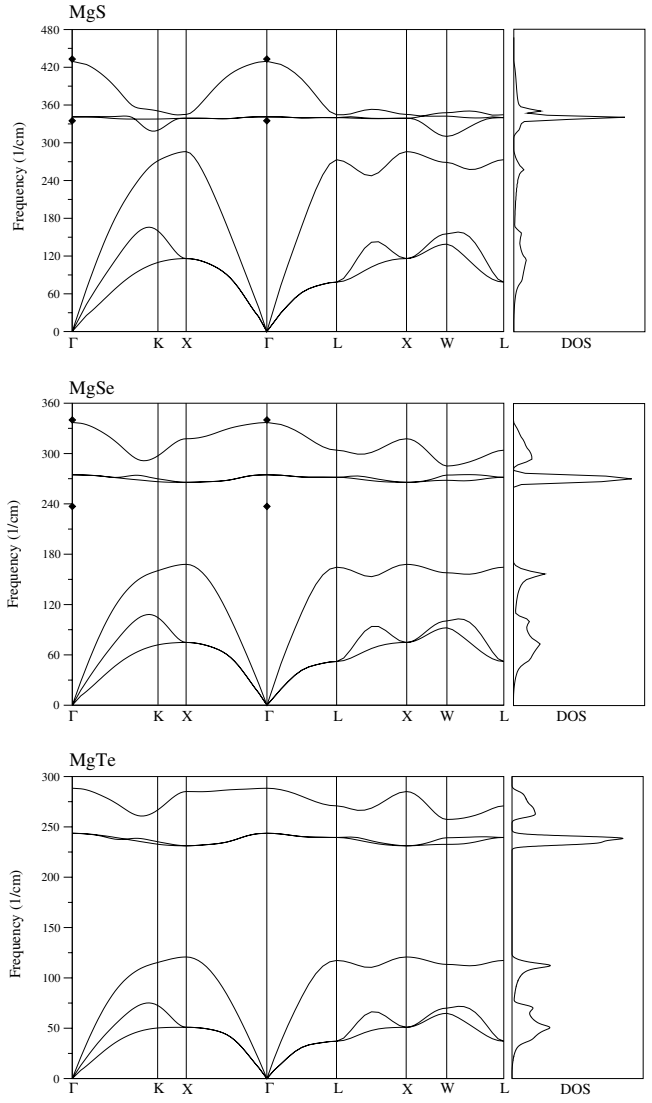

FIG. 8. Calculated phonon dispersion curves and phonon density of states for Mg chalcogenides in the zinc blende phase. Solid diamonds are experimental data from Ref. 17 for MgS and Ref. 18 for MgSe.

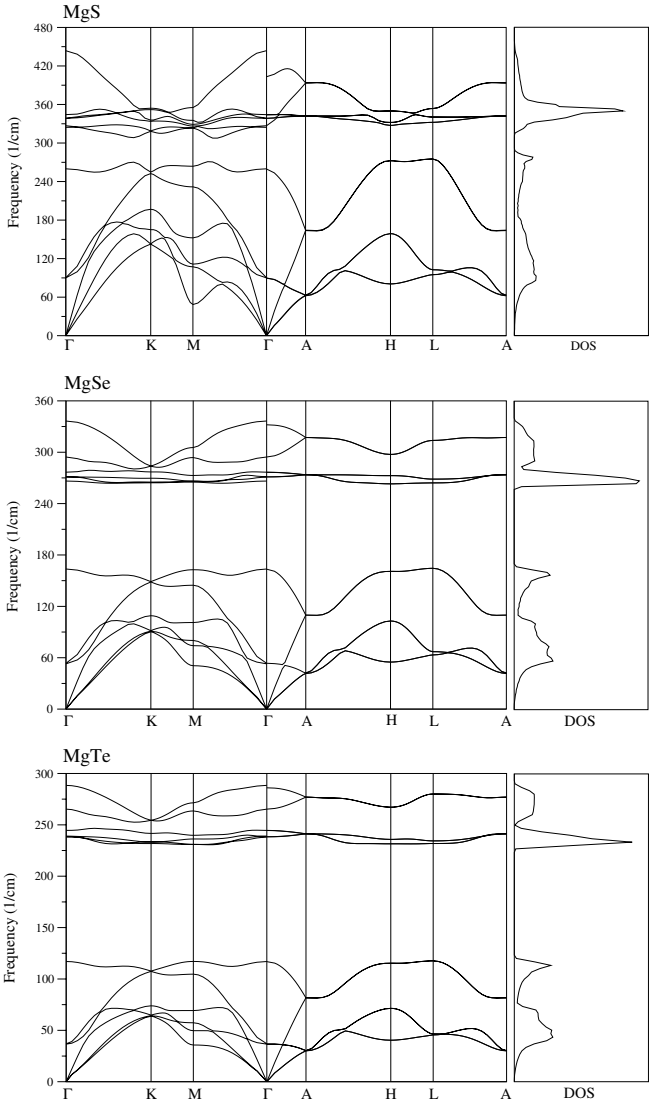

FIG. 9. Calculated phonon dispersion curves and phonon density of states for Mg chalcogenides in the wurtzite phase.

ciable angular dispersion with respect to the c axis. One long and three short bond lengths surrounding each atom in the WZ phase affect the frequency difference between the E_1(LO) and A_1(LO) phonon modes. This effect can be studied by increasing the internal geometrical parameter u from its ideal value of 0.375. The dependence of the A_1(LO) and E_1(LO) phonon modes on the internal parameter u of the WZ structure is illustrated in Fig. 12. When the internal parameter u is increased from its ideal value of 0.375, one long bond along the c axis is also increased. This change in the long bond makes the effective force constant weaker for the A_1(LO) mode, the longitudinal optical phonon mode along the c axis. Thus, the frequency of this phonon mode decreases when the internal parameter u increases from its ideal value of 0.375. On the other hand, the E_1(LO) phonon mode lies at higher frequency as the internal parameter u increases further from its ideal value of 0.375.

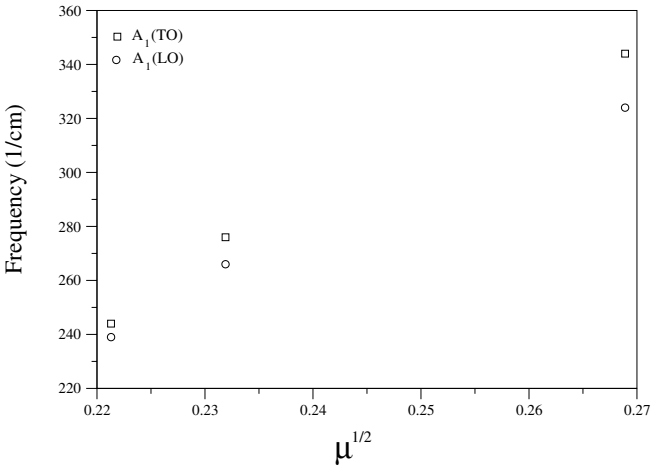

FIG. 10. The A_1(TO) and A_1(LO) phonon modes of the wurtzite MgS, MgSe, and MgTe against the square root of the reduced mass (μ) of the cation and anion.

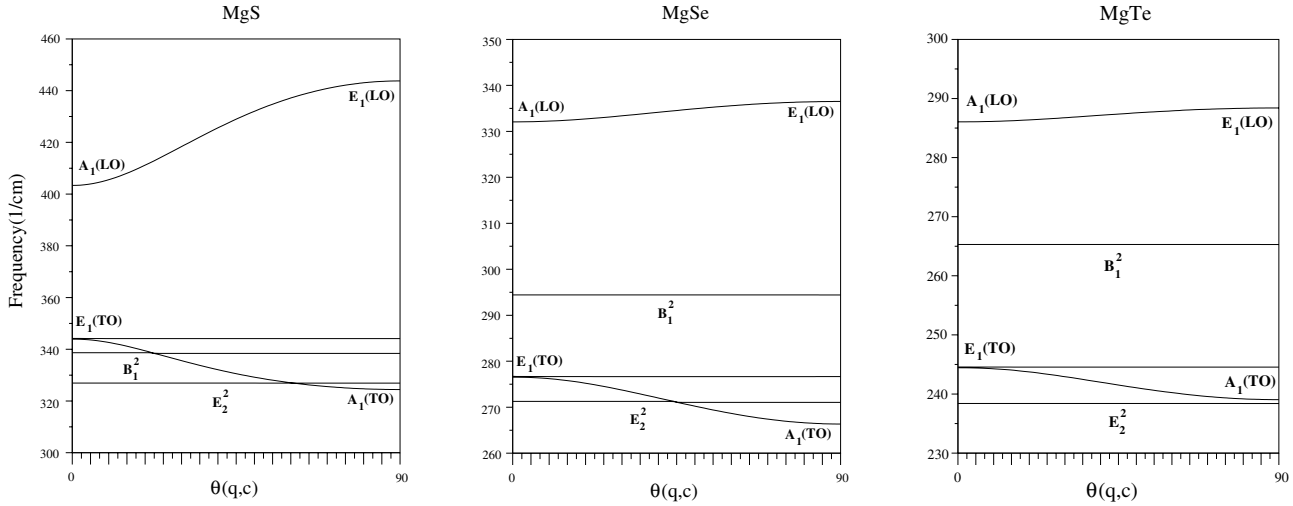

FIG. 11. Angular dependence of the zone-center phonon modes in the wurtzite structure of MgS, MgSe, and MgTe, with θ as the angle between the c axis and $\mathbf{q}\rightarrow 0$. The mode symmetries A_1, E_1, B_1, and E_2 are also indicated.

It is interesting to compare and contrast the phonon spectrum for the WZ phase with that for the ZB phase. For both structures each atom of one kind is tetrahedrally surrounded by atoms of other chemical species. With reference to the middle to a straight bond along the [111] direction, one structure can be obtained by locally rotating the other by 60°. However, in contrast to the ZB structure, the WZ structure has two structural degrees of freedom: the internal parameter u and the axial ratio c/a. The extent of the Brillouin zone in the WZ phase along the [111] direction is only half of that in the ZB phase. Thus, the lower and upper B_1 phonon modes in the WZ structure can be identified with the LA and LO phonon modes of the ZB structure at the L symmetry point. In addition to this, the frequencies of E_2^1 and E_2^2 phonon modes are very close to those of TA and TO phonon modes at the L point in the ZB structure. For example, the corresponding frequencies for the ZB MgSe are found to be 52 cm^{-1} and 271 cm^{-1} which compare very well with the E_2^1 and E_2^2 frequencies of 53 cm^{-1} and 271 cm^{-1}. Moreover, the zone-center TO and LO frequencies of the ZB structure can be related to A_1 and E_1 phonon modes by using $\omega_{T0}=[\omega(E_1(\mathrm{TO}))+\omega(A_1(\mathrm{TO}))]/2.0$ and $\omega_{L0}=[\omega(E_1(\mathrm{LO}))+\omega(A_1(\mathrm{LO}))]/2.0$. From these relations, the zone-center TO (LO) phonon modes are determined to be 334 cm^{-1} (423 cm^{-1}) for MgS, 271 cm^{-1} (334 cm^{-1}) for MgSe, and 241 cm^{-1} (287 cm^{-1}) for MgTe. These values are in good agreement with the calculated ZB phase TO (LO) phonon modes of 341 cm^{-1} (429 cm^{-1}), 274 cm^{-1} (337 cm^{-1}), and 243 cm^{-1} (288 cm^{-1}) for MgS, MgSe, and MgTe, respectively.

4. Nickel arsenide phase

As can be seen from Fig. 13, there are 12, 8, and 6 phonon modes along the Γ-K (or Γ-M), Γ-A, and A-H (H-L and L-A) symmetry directions as found in the WZ structure. Quite different from the WZ phase of MgS and MgSe, there is not a clear gap in the phonon spectrum and density of

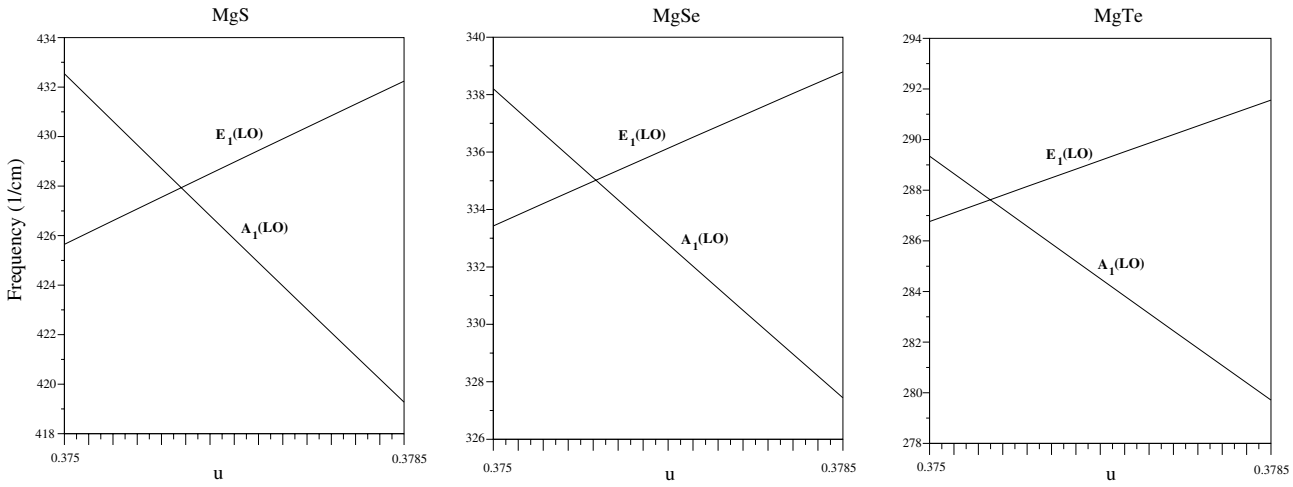

FIG. 12. The effect of the internal parameter u on the A_1(LO) and E_1(LO) phonon modes in the wurtzite phase of MgS, MgSe, and MgTe.

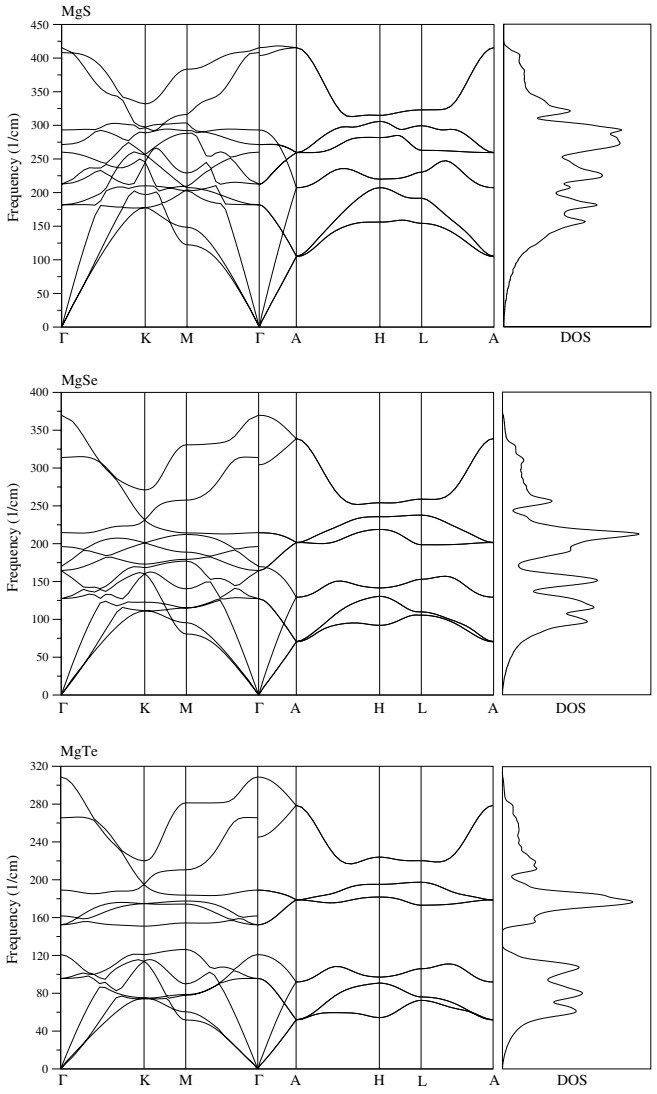

FIG. 13. Calculated phonon dispersion curves and phonon density of states for Mg chalcogenides in the nickel arsenide phase.

states for the NiAs phase of these semiconductors. The gap in the NiAs phonon spectrum of MgTe is also smaller than the corresponding gap in the phonon spectrum of its WZ phase. This difference can be related to different atomic bondings in these structures. For this structure, we will use the same mode labeling as for the WZ structure. Thus, zone-center phonon modes for the NiAs phase of Mg chalcogenides are presented in Table VI according to their *A*, *B*, and *E* characters.

When considering the four structural phases for the three Mg chalcogenides, the highest phonon-mode frequency is found to be similar (and higher) for the WZ and ZB phases and similar (and slightly lower) for the NiAs and RS phases.

D. Analysis of differences between the ZB and WZ phases of MgTe

It was stated earlier that we cannot confidently differentiate between the relative stabilities of the ZB and WZ phases of MgTe. From Tables IV and V it is clear that MgTe is a direct band gap material in both the ZB and WZ phases, with very similar valence band width, ionicity gap, and fundamental band gap. These two phases cannot be identified on the basis of the electronic (and optical) band gap. However, the two phases can be differentiated on the basis of the electronic density of states: from Figs. 3 and 4 it can be seen that, compared to the ZB phase, there is a richer structure in the entire valence band region of the WZ phase.

Furthermore, it is clear from Figs. 8 and 9 that the ZB and WZ phases of MgTe are characterized by similar acoustic phonon bandwidth, acoustic-optical band gap, and the bandwidth of the optical phonon branches (upper optical branches in the case of WZ). Thus these features do not differentiate between the two phases. However, while there is a gap of 10 cm^{-1} in the optical range for the ZB phase, no clear gap exists in the upper optical range for the WZ phase. Such an amount of gap is measurable experimentally and thus should be considered as a fingerprint of the ZB phase of MgTe. Thus, while the total energy analysis does not help differentiate the ZB and WZ polytypes of MgTe, we have identified measurable differences in the electronic density of states as well as in the phonon density of states for the two phases.

Finally, the LDA phonon results presented above do not change by more than 8% when a generalized gradient approximation[43] is employed. We have compared our LDA and GGA phonon results for the RS and ZB phases of Mg chalcogenides at the zone edges of *X* and *L* in Table VII. Such changes are within typical experimental error margins. Thus, it is fair to say that the LDA results are of as good a quality as the GGA results are.

IV. SUMMARY

We have presented well converged *ab initio* studies of the ground-state, electronic, and vibrational properties of Mg chalcogenides crystallizing in rocksalt, zinc blende, wurtzite, and nickel arsenide structures by employing a first-principles scheme, based on the application of the plane-wave pseudopotential method within the density functional scheme and a linear response scheme. Some trends in these properties have been established.

Our results for total energy calculations indicate that the rocksalt structure is the most stable phase for MgS and MgSe, while the ground-state phase for MgTe is found for the nickel arsenide structure. The electronic band structure results for the zinc blende and wurtzite phases of these semiconductors are very similar to each other due to similar tetrahedral bonds in these structures, while the results for the rocksalt and nickel arsenide phases are similar to each other due to similar octahedral bonds in these structures. The phonon dispersion curves and density of states for the three materials in the four phases have been calculated and discussed in detail. Although the zinc blende and rocksalt structures have the same number of atoms per unit cell, due to differences in atomic coordination numbers, there are clear differences in the phonon density of states. Similarly, despite the same number of atoms per unit cell, due to different coordination numbers, the phonon densities of states for the wurtzite and nickel arsenide phases are quite different. In general

TABLE VII. Comparison of LDA and GGA (in parentheses) phonon results for RS and ZB phases of Mg chalcogenides at the zone edges of *X* and *L*. Frequencies are given in cm^{-1}. We note that our GGA lattice constants for the RS and ZB phases are typically 1.5%–2% higher than the corresponding LDA values.

Structure/symmetry point	Material	TA	LA	TO	LO
RS/*X*	MgS	119 (129)	179 (187)	271 (258)	308 (295)
	MgSe	72 (79)	112 (117)	200 (194)	221 (212)
	MgTe	37 (47)	66 (75)	162 (166)	176 (178)
RS/*L*	MgS	177 (174)	293 (288)	207 (195)	364 (354)
	MgSe	96 (98)	169 (166)	189 (180)	328 (320)
	MgTe	56 (65)	120 (120)	172 (167)	282 (278)
ZB/*X*	MgS	116 (124)	285 (274)	339 (315)	345 (330)
	MgSe	75 (79)	168 (161)	266 (250)	317 (304)
	MgTe	51 (56)	121 (118)	231 (223)	285 (276)
ZB/*L*	MgS	79 (83)	273 (269)	340 (317)	344 (326)
	MgSe	52 (54)	164 (160)	272 (256)	303 (291)
	MgTe	37 (39)	117 (116)	239 (230)	271 (264)

the gap in the density of states for the nickel arsenide phase is smaller than that for the wurtzite phase. Thus the present work clearly points out that the lattice dynamics of a crystal is governed by atomic masses as well as atomic coordination number.

The relative stabilities of the polytypic ZB and WZ phases of MgTe cannot be confidently established from total energy calculations alone. Although these two phases cannot be differentiated on the basis of the electronic (and optical) band gap, these can be differentiated on the basis of details of the electronic density of states. These two phases of MgTe can also be differentiated from an examination of the phonon density of states in the optical range.

ACKNOWLEDGMENTS

This work was supported by the Scientific and Technical Research Council of Turkey (TUBİTAK) and the Engineering and Physical Sciences Research Council of the United Kingdom (EPSRC).

[1] M. A. Hasse, J. Qiu, J. M. DePuydt, and H. Cheng, Appl. Phys. Lett. **59**, 1272 (1991).
[2] S. Albin, J. D. Satira, D. L. Livingston, and T. A. Shull, Jpn. J. Appl. Phys., Part 1 **31**, 715 (1992).
[3] M. W. Wang, M. C. Phillips, J. F. Swenberg, E. T. Yu, J. O. McCaldin, and T. C. McGill, J. Appl. Phys. **73**, 4660 (1993).
[4] M. W. Wang, J. F. Swenberg, M. C. Phillips, E. T. Yu, J. O. McCaldin, R. W. Grant, and T. C. McGill, Appl. Phys. Lett. **64**, 3455 (1994).
[5] H. Okuyama, K. Nakano, T. Miyajima, and K. Akimoto, J. Cryst. Growth **117**, 139 (1992).
[6] A. Waag, H. Heinke, S. Scholl, C. R. Becker, and G. Landwehr, J. Cryst. Growth **131**, 607 (1993).
[7] L. Konczenwicz, P. Bigenwal, T. Cloitre, M. Chibane, R. Ricou, P. Testuo, O. Briot, and R. L. Aulombard, J. Cryst. Growth **159**, 117 (1996).
[8] W. Klemm and K. Wahl, Z. Anorg. Allg. Chem. **266**, 289 (1951).
[9] H. Mittendorf, Z. Phys. **183**, 113 (1965).
[10] T. Li, H. Luo, R. G. Greene, A. L. Ruoff, S. S. Trail, and F. J. DiSalvo, Phys. Rev. Lett. **74**, 5232 (1995).
[11] P. E. Van Camp, V. E. V. Doren, and J. L. Martins, Phys. Rev. B **55**, 775 (1997).
[12] A. Chakrabarti, Phys. Rev. B **62**, 1806 (2000).
[13] D. Rached, N. Benkhettou, B. Soudini, B. Abbar, N. Sekkal, and M. Driz, Phys. Status Solidi B **240**, 565 (2003).
[14] F. Drief, A. Tadjer, D. Mesri, and H. Aourag, Catal. Today **89**, 11343 (2004).
[15] A. Fleszar, Phys. Rev. B **64**, 245204 (2001).
[16] C. Y. Yeh, Z. W. Lu, S. Froyen, and A. Zunger, Phys. Rev. B **46**, 10086 (1992).
[17] D. Wolverson, D. M. Bird, C. Bradford, K. A. Prior, and B. C. Cavenett, Phys. Rev. B **64**, 113203 (2001).
[18] D. Huang, C. Jin, D. Wang, X. Liu, J. Wang, and X. Wang, Appl. Phys. Lett. **67**, 3611 (1995).
[19] A. M. Hofmeister, E. Keppler, and A. K. Speck, Mon. Not. R. Astron. Soc. **345**, 16 (2003).

[20] P. K. Jha and M. Talati, Phys. Status Solidi B **239**, 291 (2003).
[21] N. Troullier and J. L. Martins, Phys. Rev. B **43**, 1993 (1991).
[22] D. M. Ceperley and B. J. Alder, Phys. Rev. Lett. **45**, 566 (1980).
[23] S. Baroni, P. Giannozzi, and A. Testa, Phys. Rev. Lett. **58**, 1861 (1987).
[24] S. Baroni, S. de Gironcoli, A. Dal Corso, and P. Giannozzi, Rev. Mod. Phys. **73**, 515 (2000).
[25] S. Baroni, A. Dal Corso, S. de Gironcoli, and P. Giannozzi, http://www.pwscf.org
[26] F. D. Murnaghan, Proc. Natl. Acad. Sci. U.S.A. **50**, 697 (1944).
[27] R. W. G. Wyckoff, *Crystal Structures* (Wiley, New York, 1963).
[28] *Crystal Data Vol. II: Inorganic Compounds*, edited by J. H. Donnay and H. M. Ondik (U.S. Department of Commerce, Washington, DC, 1972).
[29] S. G. Lee and K. J. Chang, Phys. Rev. B **52**, 1918 (1995).
[30] P. E. V. Camp and V. E. V. Doren, Int. J. Quantum Chem. **55**, 339 (1995).
[31] S. J. You, B. I. Min, and A. J. Freeman, Phys. Status Solidi B **241**, 1413 (2004).
[32] S. J. Jenkins, G. P. Srivastava, and J. C. Inkson, Phys. Rev. B **48**, 4388 (1993).
[33] K. S. Upadhyaya, M. Yadav, and G. K. Upadhyaya, Phys. Status Solidi B **229**, 1129 (2002).
[34] G. Raunio, L. Almqvist, and R. Stedman, Phys. Rev. **178**, 1496 (1969).
[35] M. T. Dove, *Introduction to Lattice Dynamics* (Cambridge University Press, Cambridge, England, 1993).
[36] P. Villars and L. D. Calvert, *Pearson's Handbook of Crystallographic Data for Intermetallic Phases* (American Society of Metals, Metals Park, OH, 1985).
[37] C. B. Chaudhuri, G. Pari, A. Mookerjee, and A. K. Bhattacharyya, Phys. Rev. B **60**, 11846 (1999).
[38] G. Kalpana, B. Palanivel, R. M. Thomas, and M. Rajagopalan, Physica B **222**, 223 (1996).
[39] V. S. Stepanyuk, A. A. Grigorenko, A. A. Katsnelson, O. V. Farberovich, A. Szasz, and V. V. Mikhailin, Phys. Status Solidi B **174**, 289 (1992).
[40] M. Rabah, B. Abbar, Y. Al-Douri, B. Bouhafs, and B. Sahraoui, Mater. Sci. Eng., B **100**, 163 (2003).
[41] H. Okuyama, K. Nakano, T. Miyajima, and K. Akimoto, Jpn. J. Appl. Phys., Part 2 **30**, L1620 (1991).
[42] S. G. Parker, A. R. Reinberg, J. E. Pinnell, and W. C. Holton, J. Electrochem. Soc. **118**, 979 (1971).
[43] J. P. Perdew, K. Burke, and M. Ernzerhof, Phys. Rev. Lett. **77**, 3865 (1996).